World Scientific
www.worldscientific.com

On the thermally-driven gas flow through divergent micro/nanochannels

Mohammad Sajjad Mozaffari* and Ehsan Roohi†

High Performance Computing (HPC) Laboratory
Department of Mechanical Engineering
Ferdowsi University of Mashhad
P.O. Box 91775-1111, Mashhad, Iran
*sajjad.mozaffari@gmail.com
†e.roohi@ferdowsi.um.ac.ir

A detailed study on thermally driven flows through divergent micro/nanochannels is presented. Rarefied gas flow behavior and thermal mass flow rate were investigated with different divergence angles ranging between 0° and 7° at two aspect ratios ($AR = L/H_{in} = 6, 20$) using particle-based direct simulation Monte-Carlo (DSMC) method. We compare our DSMC solutions for normalized thermal mass flow rate with the numerical solution of the Boltzmann–Krook–Walender (BKW) model and Bhatnagar–Gross–Krook (BGK) model and asymptotic theory over a wide range of Knudsen number in the transition regime. The flow field properties including Mach number, pressure, overall temperature and magnitude of shear stress are examined in detail. Based on our analysis, we observed an approximately constant velocity and pressure distribution at a microchannel with a small opening angle. Our results also demonstrate that the heat lines from weakly nonlinear form of Sone constitutive law and DSMC show good agreement at low Knudsen numbers. Moreover, we show that the effect of divergence angle is influential in increasing normalized thermal mass flow rate at early transition regime.

Keywords: Divergent micro/nanochannel; thermally-driven flows; rarefied gas flow; direct simulation Monte Carlo (DSMC).

PACS Nos.: 47.61.–k, 47.45.–n, 05.70.–a, 02.70.–c.

1. Introduction

There is a renewed interest in development of thermally driven flow in micro/nano-electro-mechanical systems (MEMS/NEMS). It is crucial to understand the gas flow behavior through geometry with sudden or gradual expansion. These geometries could find applications in microscale systems such as microactuators, microturbines, gas chromatographs, micro air vehicles, MEMS devices and micromolecular

---

† Corresponding author.

compressors.[1–4] Most of the earlier studies focused on microchannels with nonuniform cross-sections conducting liquid flows.[5–8] To review works on gas flows, one could note work of Varade *et al.*[9] who performed an experimental and numerical study on gaseous flow at slip regime through divergent microchannels. They showed that the pressure drop, centerline velocity, and wall shear decrease with an increase in divergence angle for their range of study. Hemadri *et al.*[10] studied rarefied gas flow in converging and diverging cross-sections. They observed Knudsen minimum for the first time in a microchannel of varying cross-section. They investigated the effect of geometrical cross-section and fluid properties on the Knudsen minimum. They also found that the values of Knudsen number and the minimum mass flow rate are the same for both converging and diverging cross-sections at the location of Knudsen minimum. They indicated the absence of any flow preference at high Knudsen numbers when the flow is subjected to converging and diverging orientations of the microchannel.[11]

In addition to the pressure gradient, temperature could induce flow in micro/ nanoscale geometries. Due to a nonuniform wall temperature distribution applied to the channel walls, flow could start creeping from the cold region toward the hot one. This flow is called thermal creep/transpiration flow.[12] A traditional application of thermally-driven flow is Knudsen compressor/pump which works without any moving part under rarefied condition. Knudsen built a thermally-driven pump operating according to the thermal creep/transpiration phenomenon.[13] Knudsen pump could find applications in MEMS/NEMS such as gas sensors, fuel cells, and lab on a chip.[14–16] Thermal creep/transpiration problems were studied by several researchers during the past[17–19] and recent years.[15,20,21] Alexeenko *et al.*[15] investigated the effects of wall temperature distribution applied to a two-dimensional finite length microchannel. They examined three wall temperature distributions: linear, stepwise, and a nonmonotonic profile typical for a radiantly heated Knudsen compressor's membrane and compared BGK and ES and DSMC solutions. Akhlaghi *et al.*[20] considered flow between two parallel plates with a linear wall temperature gradient applied to their surfaces at isobaric inlet/outlet condition. They reported mass flow rate dependency on the wall temperature and derived analytical expressions for the mass flux. Tatsios *et al.*[21] considered the associated pumping effects through extended channels with linearly diverging or converging cross-sections. They parametrized mass flow rate and the induced pressure difference between the channel inlet and outlet in terms of geometrical and operational data including the channel inclination and the inlet pressure.

The impetus for this work is to investigate thermal creep effect on fluid flow behavior and the mass flow rate of the rarefied gas flow through micro/nanoscale channels over a wide range of Knudsen numbers. We used DSMC method as our simulation method to accurately simulate rarefied gas. The effect of geometrical parameters such as wall divergence angle and aspect ratio are considered in detail. For the first time, we will describe mass flow rate dependence on the divergence angle under thermal creep conditions.

2. DSMC Solver

Based on the continuum approximation, the Navier–Stokes–Fourier (NSF) equations break down when the mean free path (λ) of the molecule becomes comparable to the characteristic length (L) of the geometry conducting the gas. The nondimensional parameter, Knudsen number ($Kn = \lambda/L$) is usually considered to classify the gas flow rarefaction regimes, including continuum regime ($Kn < 0.001$), slip flow regime ($0.001 \leq Kn < 0.1$), transition flow regime ($0.1 \leq Kn < 10$) and free molecular regime ($Kn \geq 10$). Direct simulation Monte-Carlo (DSMC) is widely employed to accurately and efficiently model flow fields in all rarefaction regimes. This method, developed by Bird,[22] is based on the molecular simulation of dilute gas flows. The DSMC procedure consists of the movement of particles, indexing of particles in cells, particles collision and sampling. In this method, every simulator particle represents a large number of real gas molecules. The number of particles must be large enough to represent the velocity distribution of real gas molecules. Here, our employed molecular collision model is variable hard sphere (VHS). VHS model, introduced by Bird, is based on a variable cross-section relation with relative velocities for the colliding pairs.[23,24] There are different collision schemes in DSMC, i.e. time counter (TC), Null collision, Ballot box, Modified Nanbu, Majorarant frequency scheme (MFS), No time counter (NTC), Bernoulli Trials, Simplified and Generalized Bernoulli Trials, for more details see Refs. 25–28. In this paper, the collision pairs are selected based on the standard NTC collision method. Diffuse reflection model is chosen for all solid surfaces. An improved version of the DSMC solver of open source C++ CFD toolbox OpenFOAM, dsmcFoam, is employed.[29–31] There are several possible ways to check the convergence of the DSMC simulations, here we considered convergence of mass flow rate at various sections of the channel, i.e. mass flow rate is calculated and once it becomes equal at various sections of the channel, the solution is considered as converged. However, the simulations were continued for a much longer time to suppress statistical scatters in the DSMC results.

3. Divergent Channel Geometry

The micro divergent channel with isobaric inlet/outlet condition is depicted in Fig. 1. Nitrogen gas with properties listed in Table 1, is considered at various Knudsen numbers ranging between 0.1 and 10. The inlet gas temperature (T_{in}) value was kept at $300\,K$ and the inlet gas pressure (p_{in}) was prescribed for each case based on the corresponding Knudsen number and the ideal gas law, see Table 2. Temperature-driven flow is produced via applying a linear wall temperature distribution as $\Delta T_{wall}/T_{in} = (T_{out} - T_{in})/T_{in}$ implemented over walls. The height of inlet channel is $0.4\,\mu m$ and aspect ratios ($AR = L/H_{in}$) 6 and 20 is considered. Lower Kn cases considered in this work correspond to microscale channels ($H = 75\,\mu m$) but higher Kn cases ($Kn > 1$) correspond to nanoscale geometries with an inlet height of $75\,nm$.
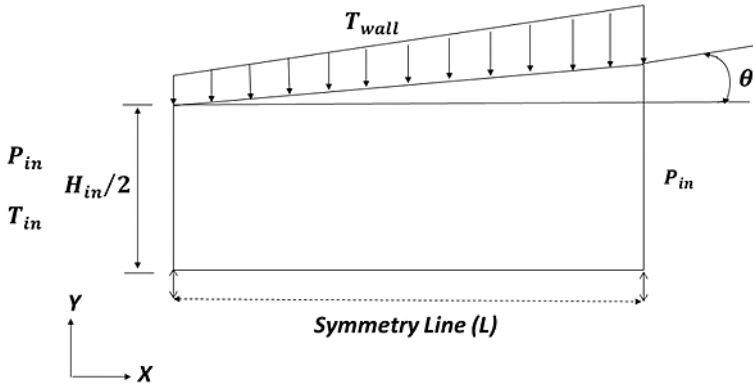
Fig. 1.   Micro/nanochannel geometry and imposed boundary condition.

Table 1.   Nitrogen gas properties.[22]

Gas	Mass (kg)	Viscosity index	Diameter (m)	Degree of freedom
N_2	46.5×10^{-27}	0.74	4.17×10^{-10}	5

Table 2.   Inlet pressure at each inlet Knudsen number.

Kn	Inlet pressure (kPa)
0.1	134.031
0.2	67.015
1	13.403
5	2.680
10	1.340

4. DSMC Simulation Accuracy

4.1. *Cell size*

When the cell size in physical space is large, macroscopic gradients are typically underpredicted. According to past studies, in an area with large gradients, the ratio of cell dimension to local mean free path should not be higher than 1/3 in the gradient direction.[32] Figure 2 shows the results of grid study test using four grids. We investigated Mach number (Ma), normalized pressure (P/P_{in}), normalized overall temperature (T/T_{in}) and normalized magnitude of the shear stress ($\tau^* = |\boldsymbol{\tau}|/P_{\text{in}}$), in the centerline of the channel. For nitrogen, overall temperature is defined as: $T = \frac{3T_{\text{tr}} + 2T_{\text{rot}}}{5}$, where T_{tr} and T_{rot} are translational and rotational temperatures, respectively.[22] Magnitude of the shear stress is defined as: $|\boldsymbol{\tau}| = \sqrt{2\boldsymbol{\tau} : \boldsymbol{\tau}}$, where double
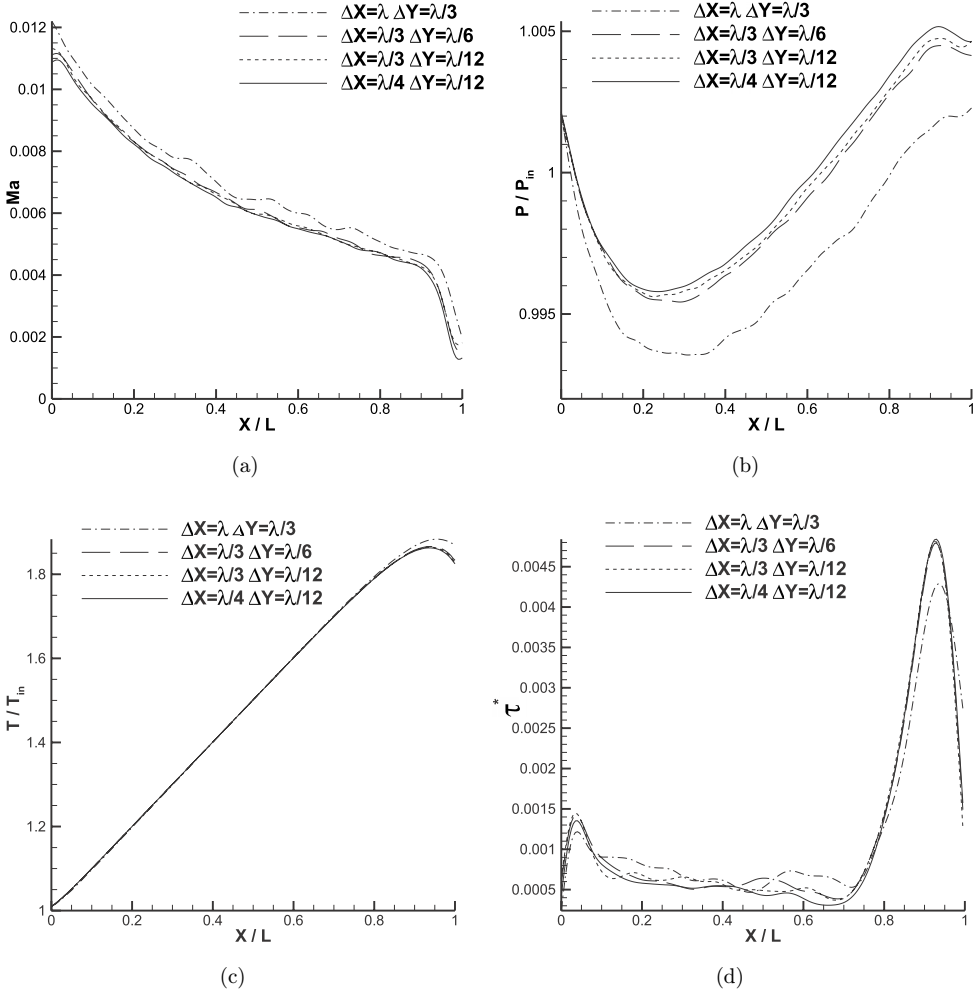
Fig. 2. Effect of cell dimension in properties at the center line of divergent micro/nanochannels. (a) Mach number, (b) nondimensional pressure, (c) nondimensional overall temperature, (d) nondimensional magnitude of the shear stress ($AR = 20, \theta = 3.5, Kn = 0.2, \Delta T_{wall}/T_{in} = 1$).

dot means component by component product and $\boldsymbol{\tau} = \langle \rho c_i c_j \rangle$, and $\langle \rangle$ means averaged value.

According to Fig. 2, the flow field is mainly affected by the cell dimension in the normal direction. Accordingly, we selected the grid using cell size of ($\lambda/3$, $\lambda/12$) which seems suitable to simulate the divergent channel accurately.

4.2. *PPC effect*

To ensure that the DSMC results do not suffer from by the shortage of simulators, we considered various numbers of particle per cell (PPC). Shu *et al.*[32] indicated that the

proper number of PPC should be as large as 20 for slip flow and 10 for transition regime. There are other values reported for the minimum required PPC, i.e. see Refs. 33 and 34. However, the required PPC value should be obtained for each test case independently. The results of PPC independence for a typical case is depicted in Fig. 3. It is observed that the results for PPC = 32 and 50 are almost similar while PPC = 32 provides a sufficient accuracy with a reduced computational cost. Therefore, we will follow the rest of this work using PPC = 32.

4.3. *Time step*

Due to the time splitting of the molecular motion and collisions in DSMC, the maximum allowable time step should be smaller than the mean molecular collision
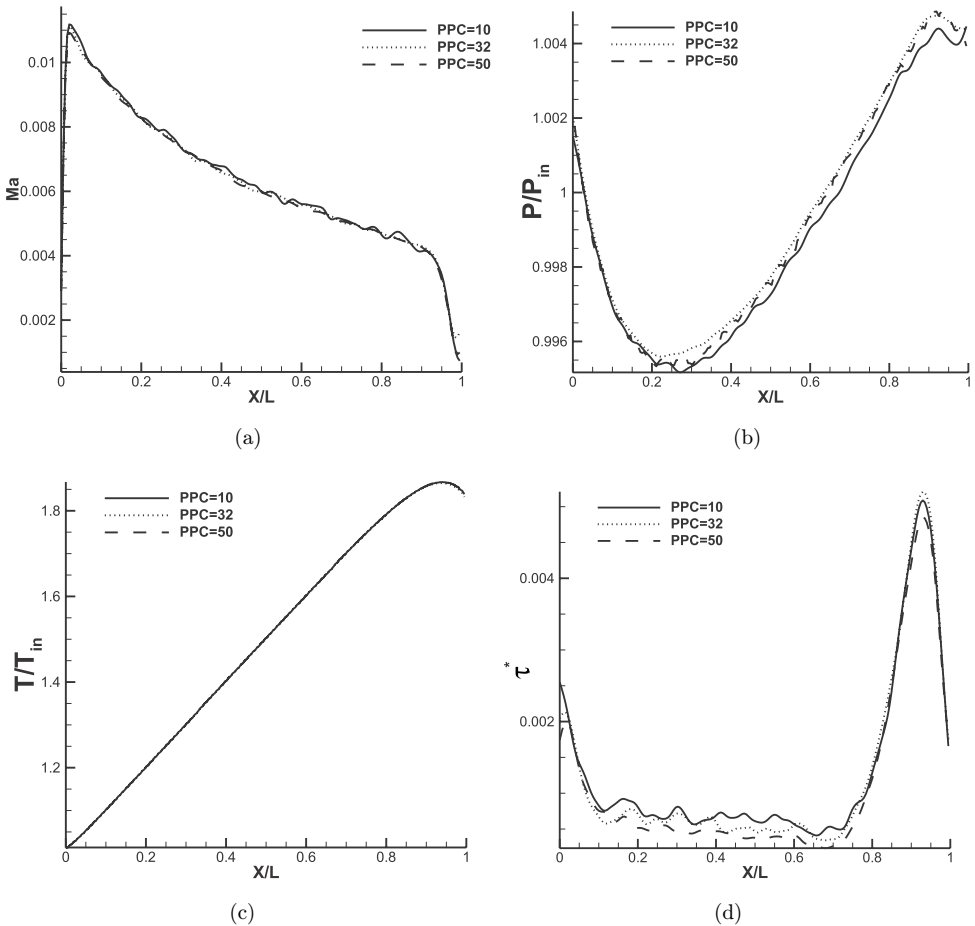

Fig. 3. Effect of PPC number in properties at the center line of divergent micro/nanochannels. (a) Mach number, (b) nondimensional pressure, (c) nondimensional overall temperature, (d) nondimensional magnitude of shear stress ($AR = 20, \theta = 3.5, Kn = 0.2, \Delta T_{wall}/T_{in} = 1$).

time defined as

$$\Delta t_c = \frac{\lambda}{V_{\text{mp}}}, \tag{1}$$

where λ and V_{mp} are mean free path of molecules and most probable molecular speed, respectively. For DSMC, the CFL number is not a stability constraint, but rather a physical requirement. Violation of this condition may produce solutions that are not physically realistic.[35] Borrowing from the traditional computational fluid dynamics (CFD), the time step due to Courant–Friedrichs–Lewy (CFL) number (Δt_{CFL}) is
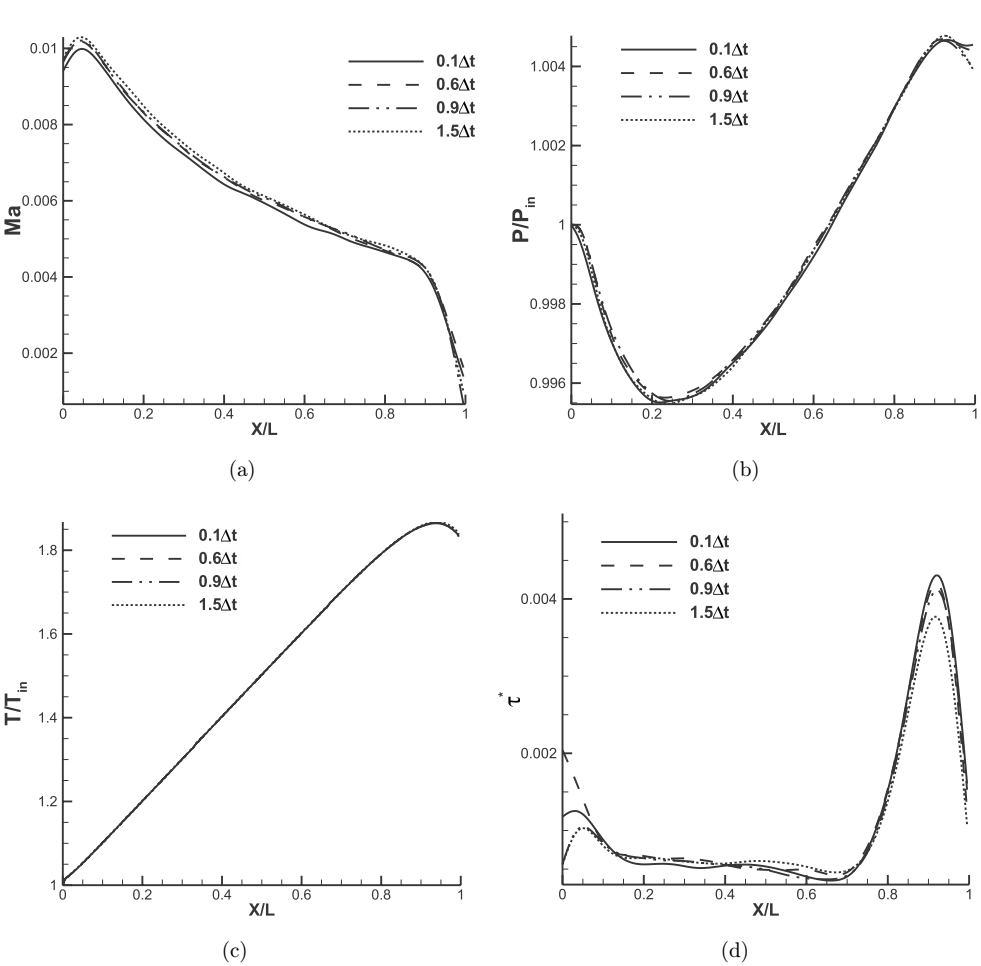

Fig. 4. Effect of time step in properties at center line of divergence microchannels. (a) Mach number, (b) nondimensional pressure, (c) nondimensional overall temperature, (d) nondimensional magnitude of shear stress ($\text{AR} = 20, \theta = 3.5, \text{Kn} = 0.2, \Delta T_{\text{wall}}/T_{\text{in}} = 1$).

given as follows:

$$\Delta t_{\mathrm{CFL}} = \frac{\mathrm{CFL} * \Delta X}{V_{\mathrm{mp}}}, \tag{2}$$

where ΔX and V_{mp} are cell dimension and most probable molecular speed, respectively. We defined the accurate time step as minimum of ΔT_{CFL} and ΔT_c with a coefficient of (α) as

$$\Delta t = \alpha * \min(\Delta t_{\mathrm{CFL}}/\Delta t_c). \tag{3}$$

In order to check the solution independence from the time step, the values of α were considered 0.1, 0.6, 0.9 and 1.5. The effect of α on the Mach number (Ma), normalized pressure, overall temperature, and magnitude of shear stress are depicted in Fig. 4. According to this figure, a time step coefficient of $\alpha = 0.6$ is recommended.

5. Results and Discussions

5.1. *Pressure distribution*

First, we report normalized pressure behavior in the channel. The static pressure is nondimensionalized with the inlet pressure magnitude. The nondimensional static pressure variations along the centerline of the micro/nanochannel are shown in Fig. 5 for four divergence angles $(0°, 1°, 3.5°, 7°)$. Figure 5(a) indicates that pressure experiences an increase followed by a decrease. The reason of increase could be temperature increase along the channel, that pressure follows it according to the equation of state; while the pressure decrease is due to pre-specified pressure at the outlet; i.e. the interior pressure decreases to match the specified magnitude at the outlet. On the other hand, the point of maximum pressure moves toward the outlet as divergence angle increases, i.e. the slope of pressure curve reduces as the divergence angle increases, i.e. compressibility effect attenuates. Even the concavity of pressure curve changes at $\theta = 7°$ and pressure falls below the inlet pressure and then increases along the channel before its final decrease as the flow approaches the channel outlet. Figures 5(b) and 5(c) show that pressure experiences a relatively constant distribution at $(\theta = 1°)$. It could be argued that a balance between the parameter which increases the pressure, i.e. wall temperature gradient, and the parameters which decrease the pressure, i.e. area increase, viscous forces, and requirement to match the outlet pressure, results in such a behavior. As the divergence angle increases, the effective length $(L_{\mathrm{side}} \times \cos\theta$, where L_{side} is the length of the side wall) of the channel reduces and decelerating contributions of area increase and viscous force decrease the pressure more. Once comparing Figs. 5(a)–5(c), it is observed that maximum pressure magnitude at $\theta = 0°$ and minimum pressure magnitude at $\theta = 7°$ increases as inlet Kn increases. The reason for the former is that thermal creep strengthens at higher Kn conditions, while the reason for the latter is stronger expansion (area effects) which reduces gas compressibility more.
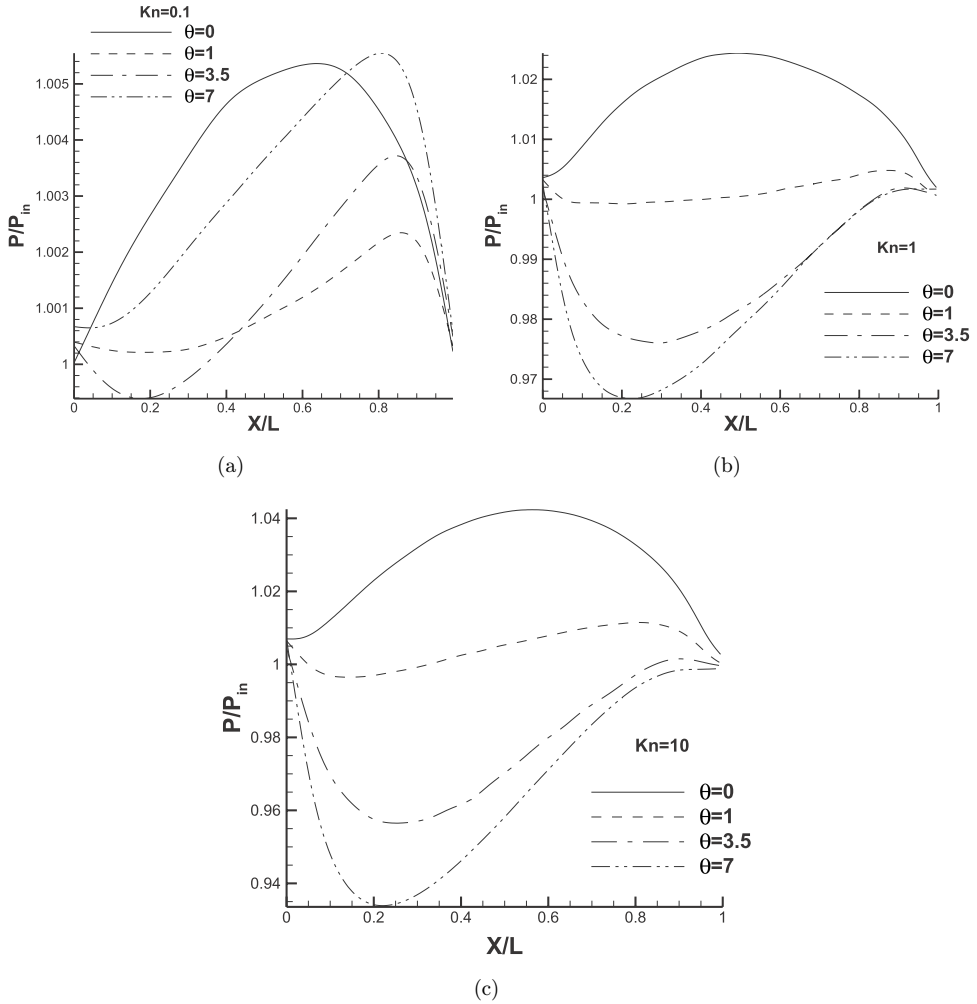
Fig. 5.   Static pressure profiles (normalized with inlet pressure) along the centerline of diverging channels with different divergence angles (a) Kn = 0.1, (b) Kn = 1, (c) Kn = 10 (AR = 20, $\Delta T_{\text{wall}}/T_{\text{in}} = 1$).

5.2. *Mach number distribution*

The variations of Mach number along the centerline of divergent micro/nanochannel at different Knudsen numbers are depicted in Fig. 6. Figure 6(a) shows that for straight channels Mach number increases and reaches its peak at the end of the geometry. This acceleration is due to thermal creep effects overcoming wall shear stress forces. The magnitude of flow Mach number increases as inlet Kn goes up because of enhanced thermal creep effects at higher Kn, i.e. thermal creep velocity linearly depends on Knudsen number.[16,36] From kinetic theory, thermal creep velocity linearly depends on the Knudsen number.
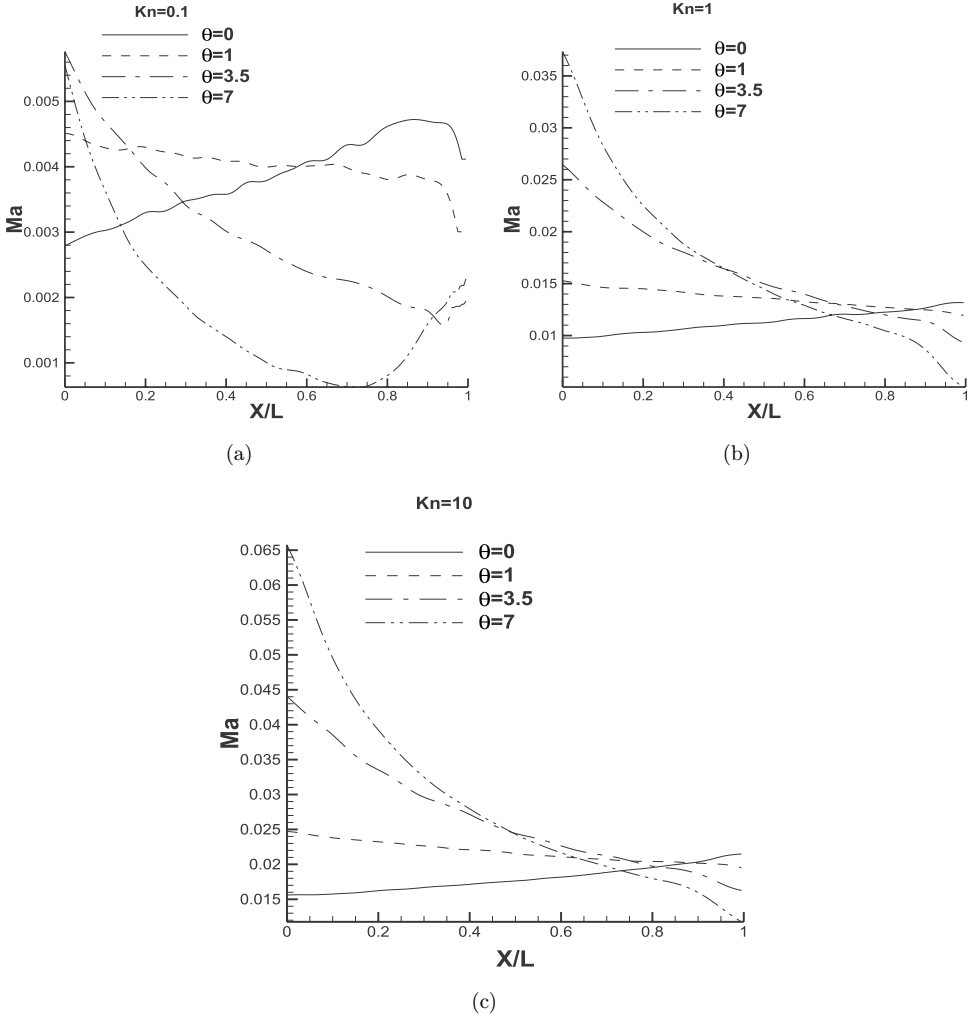
Fig. 6. Mach number distributions along the centerline of diverging channels with different divergence angles (a) Kn = 0.1, (b) Kn = 1, (c) Kn = 10 (AR = 20, $\Delta T_{\text{wall}}/T_{\text{in}} = 1$).

$$U_c \sim \text{Kn} \frac{\partial T}{\partial x^*}. \tag{4}$$

More specifically, thermal creep is proportional to Kn, temperature gradient and Knudsen layer contributions, i.e.[36]

$$U_c = -\left(\frac{\pi R T_0}{2}\right)^{1/2} \frac{\text{Kn}}{T_0} \frac{dT}{dx^*} \left[K_1 + \frac{1}{2}Y_1\left(\frac{2X_2}{\sqrt{\pi}l_0}\right)\right], \tag{5}$$

where the terms in bracket stand for Knudsen layer effects. As there are contributions from other terms in the thermal-creep driven velocity slip, e.g. Kn layer, in our

case induced Mach number was increased with more than a linear dependency once
Kn increased. At ($\theta = 1°$), Mach number distribution is decreasing due to enhanced
area expansion effects compared to straight channel; therefore, even a small diver-
gence angle could substantially alter the flow behavior. The Mach number decreases
more along the centerline of the geometry with an increase in the divergence angle of
the micro/nanochannel ($\theta = 3.5°, 7°$). For Kn ≥ 1, the Mach number distribution at
$\theta = 1°$ shows a slight decrease because of the relative balance of the viscous forces
and expansion effects with the temperature gradient, see Fig. 6(b). It should be
reminded that inlet Mach number also increases with an increase in the Knudsen
number due to the thermal creep increase.

5.3. *Temperature distribution*

Figure 7 shows nondimensional overall temperature variation along the centerline of
the micro/nanochannel at different Knudsen numbers. These figures indicate that
the overall temperature increases almost linearly through the centerline and
decreases near channel exit due to expansion cooling.[9,37] The level of expansion
cooling decreases as divergence angle increases due to stronger area effect. This
expansion cooling is the reason for pressure decrease at the end of the channel
observed in Fig. 5. At lower Kn cases, divergence angle does not affect overall
temperature distribution except at the expansion cooling region while at higher
Kn conditions overall temperature distribution slightly differs at various divergence
angles.

5.4. *Shear stress distribution*

From a molecular point of view, shear stress tensor (τ_{ij}) is proportional to $\langle c_i c_j \rangle$,
where c_i and c_j are peculiar velocities of the molecules and $\langle \rangle$ stands for averaged
values. The $\langle c_i c_j \rangle$ term indicates the transport of i-momentum per unit mass by
the j-component of the velocity.[22] Here, the magnitude of shear stress tensor, $|\boldsymbol{\tau}|$,
normalized with the inlet pressure ($\tau^* = |\boldsymbol{\tau}|/P_{\text{in}}$) is depicted in Fig. 8. Note that
normalized magnitude contains contribution of all components of the shear stress
tensor. Figure 8(a) indicates that at low Knudsen number (Kn = 0.1) shear stress
magnitude is almost constant with an increase near the terminal point of the di-
vergent microchannel. At Kn = 0.1, the increase of the divergence angle reduces
shear stress magnitude. This is because of a decrease in the effective length of the
channel with the increase of θ. As the Knudsen number increases, shear stress
magnitude initially decreases until a minimum value τ^*_{min} is attained and then
increases to a maximum value τ^*_{max}. This behavior is similar to the pressure distri-
bution for cases with higher divergence angle. Moreover, normalized magnitude of
the shear stress increases with an increase in Kn. As the particle-particle interactions
and associated relaxation of molecular velocities decrease with an increase in the
Knudsen number, a more substantial number of molecules come directly from
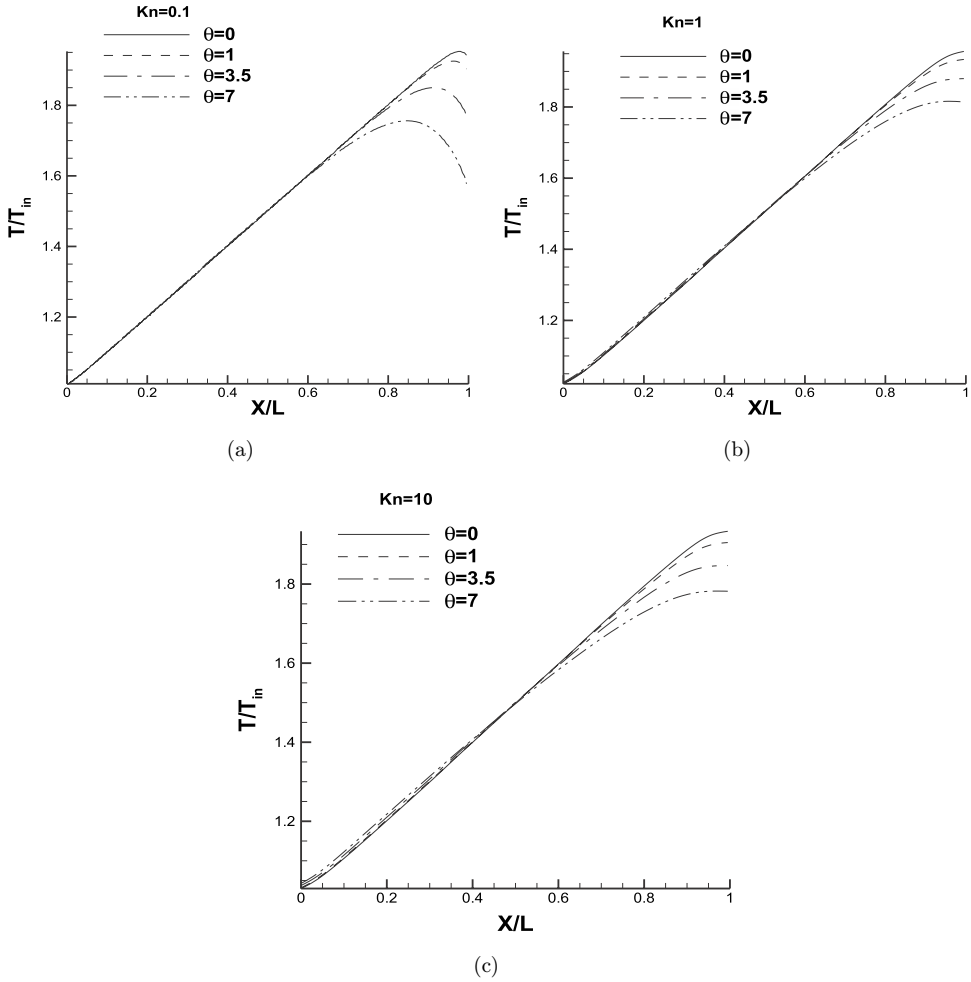
Fig. 7. Overall temperature distributions (normalized with inlet temperature) along the centreline of diverging channels with different divergence angles. (a) Kn = 0.1, (b) Kn = 1, (c) Kn = 10 (AR = 20, $\Delta T_{\text{wall}}/T_{\text{in}} = 1$).

the walls with less sharing of the gained i-momentum by other particles; as a result, the net amount of $\langle c_i c_j \rangle$ increases as Kn increases.

As a summary, three parameters affect fluid flow: dA/dx that is area expansion effects, dT/dx, which is specified wall temperature gradient and $d\tau/dx$ which is viscous effects. At $\theta = 0$, expansion effects are absent, thus temperature gradient dominates viscous effects and this leads to velocity (Mach number) increases along the micro/nanochannel. At $\theta = 1$, expansion effects start to influence the fluid behavior and almost balance other parameters, thus the pressure and velocity may have a very slight variation along the micro/nanochannel. For $\theta \geq 3.5$, expansion
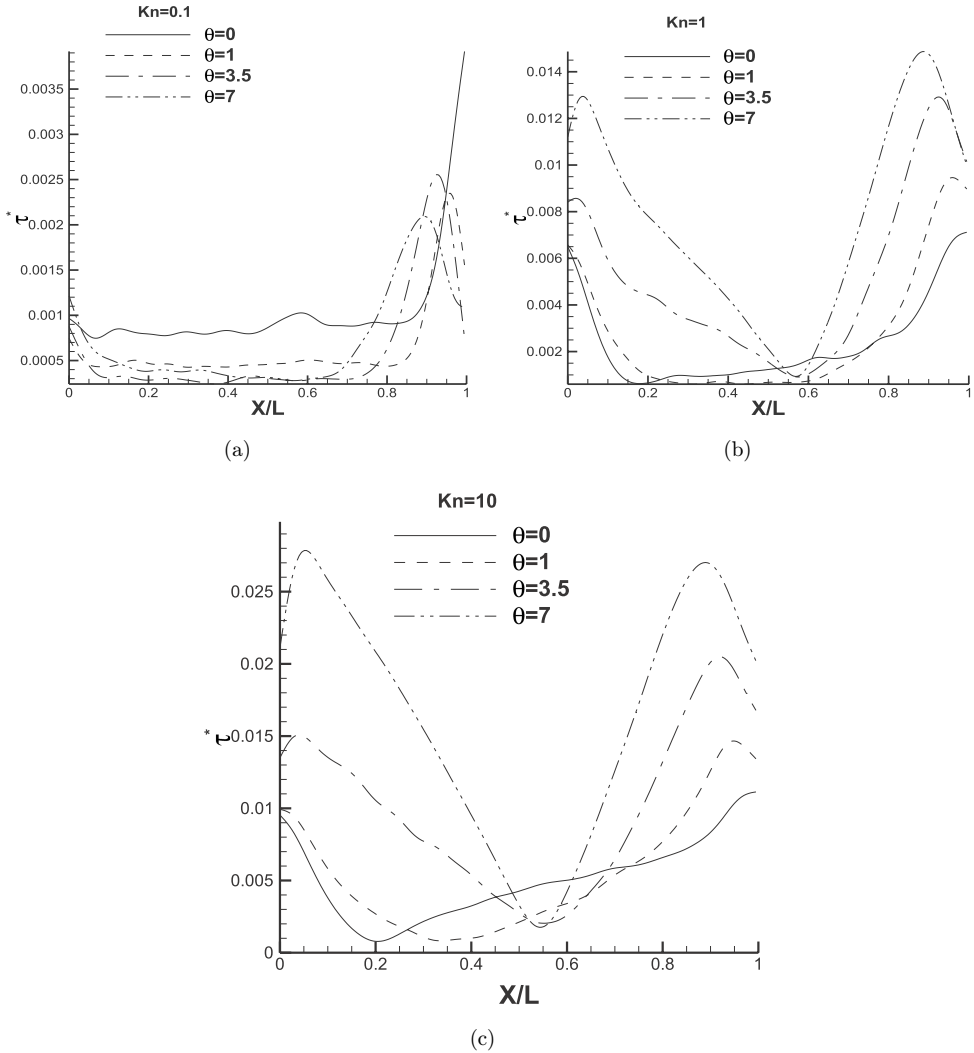
Fig. 8. Magnitude of shear stress distributions (normalized with inlet static pressure) along the centreline of diverging channels (a) $Kn = 0.1$, (b) $Kn = 1$, (c) $Kn = 10$ ($AR = 20, \Delta T_{\mathrm{wall}}/T_{\mathrm{in}} = 1$).

effects have influential contribution on the fluid behavior, as a result, the pressure and velocity decrease along divergent microchannels, see Table 3.

5.5. *Velocity profile*

The velocity profile at the mid-section of the channel is shown in Fig. 9. It shows that the flow is not developed at $Kn = 0.1$ and $\theta \geq 3.5$, see Fig. 9(a). The velocity increases with Knudsen number due to enhanced thermal creep effects. The maximum velocity occurs at the centerline of the micro/nanochannel and it depends on

Table 3.   Balances with terms influence in fluid flow behavior.

Divergence angle (θ)	dA/dx	Behavior
0	~ 0	$\frac{dT}{dx}$ dominates $\frac{d\tau}{dx}$ results in $\left(\frac{dP}{dx}, \frac{du}{dx}\right) > 0$
1	Moderate	$\frac{dT}{dx}$ balances with $\frac{dA}{dx}$ and $\frac{d\tau}{dx}$ result in $\left(\frac{dP}{dx}, \frac{du}{dx}\right) \simeq 0$
3.5, 7	Strong	$\frac{dA}{dx}$ dominates $\frac{dT}{dx}$ and $\frac{d\tau}{dx}$ and results in $\left(\frac{dP}{dx}, \frac{du}{dx}\right) < 0$

the divergence angle. The flatness of velocity profile increases with the divergence angle at higher Kn cases.

Momentum diffusivity, fluid kinetic energy, area increase, and velocity slip are parameters that influence the gas flow through the divergent channel. There is no
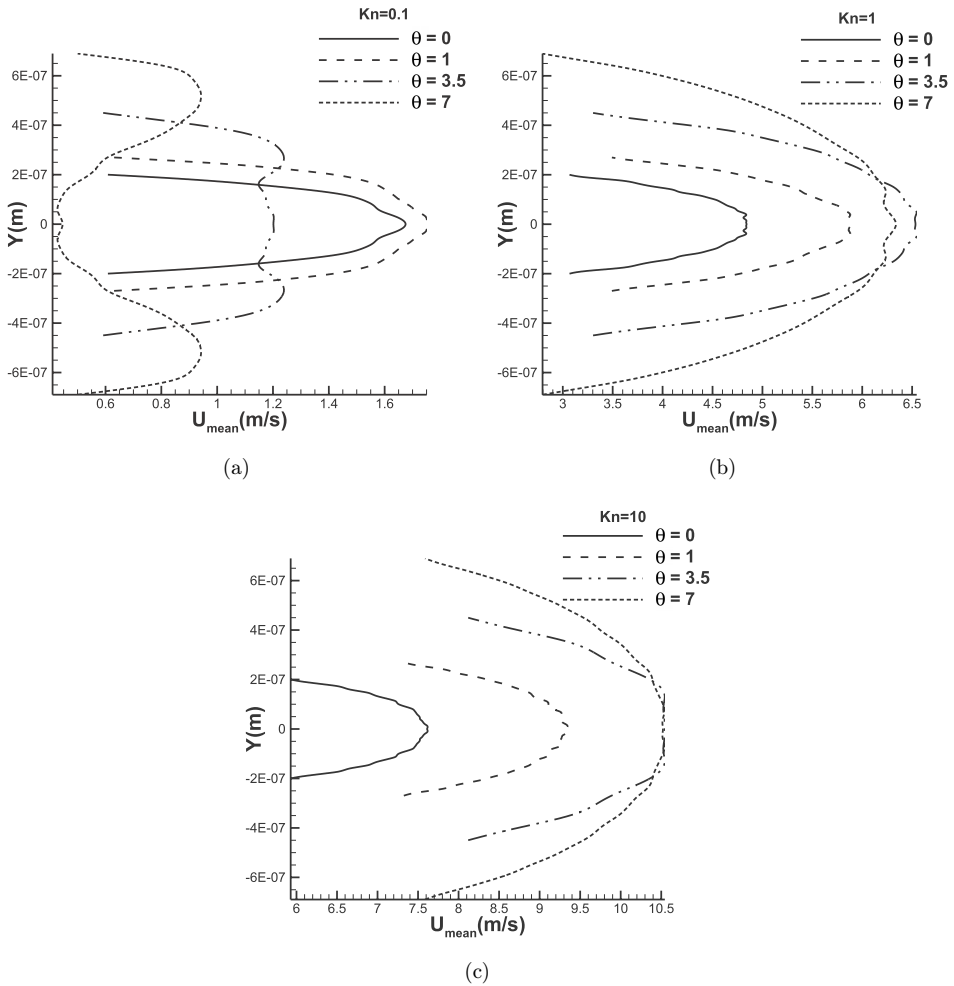

Fig. 9.   Velocity profile at $x/L = 0.5$. (a) Kn = 0.1, (b) Kn = 1, (c) Kn = 10 (AR = 20, $\Delta T_{\text{wall}}/T_{\text{in}} = 1$).

reverse flow in all cases, see Fig. 10, which depicts Mach number contour lines. Variation in cross-section may lead to reverse flow, but the effects of the velocity slip due to the thermal creep could eliminate the effect of kinetic energy.

5.6. *Slip Mach number*

Figure 11 shows the variations of the slip Mach number on the divergent micro-channel wall for different divergence angles and Knudsen numbers. The slip velocity is defined as the velocity difference between the wall and the gas adjacent to the wall. It is found that the slip velocity on the channel walls increases with an increase in the divergence angle of the channel or Knudsen number. Also, we could expect that a similar pattern occurs for the slip velocity distribution. This occurs due to the intensification of the nonequilibrium effects with Kn. The rate of the collisions between the gas molecules and the solid walls reduces under the rarefied condition which results in an increased slip velocity at higher Kn conditions.[22]

5.7. *Heat lines*

We turn to compare heat flux lines, i.e. curves that are instantaneously tangent to the heat flux vector predicted by DSMC solution with the solution of the asymptotic theory of the Boltzmann equation for weakly nonlinear flow (Sone's equation).[36]
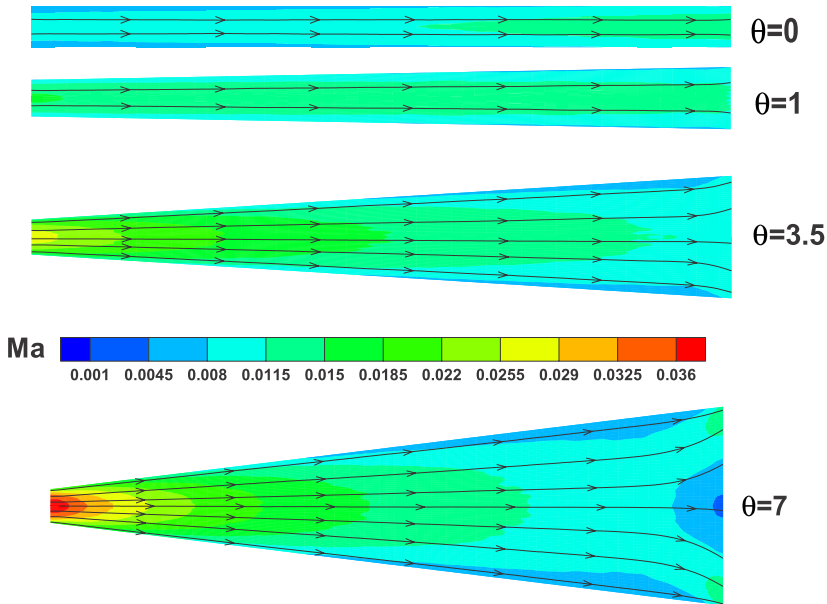

Fig. 10. (Color online) Mach number distribution for case with $(\mathrm{AR} = 20, \mathrm{Kn} = 1, \Delta T_{\mathrm{wall}}/T_{\mathrm{in}} = 1)$ at various divergence angles.
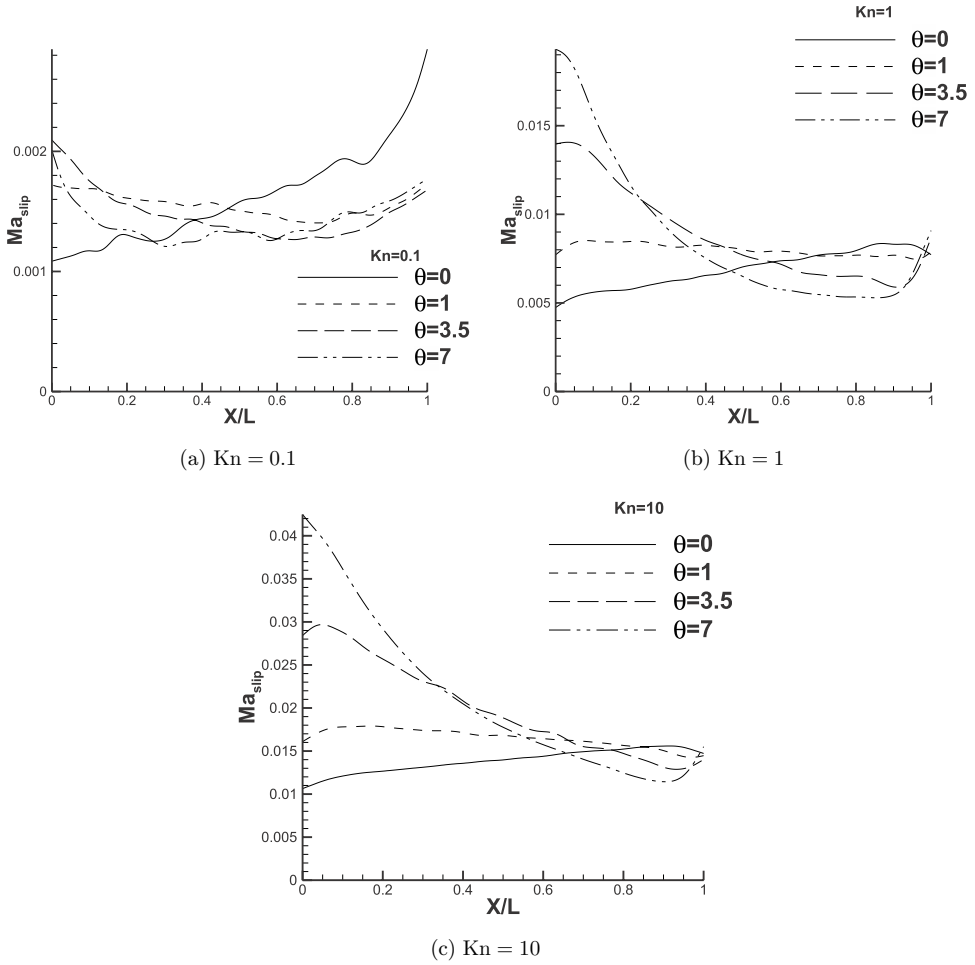
Fig. 11.   Slip velocity distributions along the surfaces of diverging channels with different divergence angles (AR = 20, $\Delta T_{\text{wall}}/T_{\text{in}} = 1$).

In these equations, the heat flow vector $\mathbf{Q_{iS}}$ is given as follows:

$$\mathbf{Q_{iS}} = \text{Kn}^{**}\mathbf{Q_{iS1}} + \text{Kn}^{**2}\mathbf{Q_{iS2}} + \text{Kn}^{**3}\mathbf{Q_{iS3}}, \tag{6}$$

$$\mathbf{Q_{iS1}} = 0, \tag{7}$$

$$\mathbf{Q_{iS2}} = -\frac{5}{4}\gamma_2 \frac{\partial \tau_s^{**}}{\partial x_i}, \tag{8}$$

$$\mathbf{Q_{iS3}} = -\frac{5}{4}\gamma_2 \frac{\partial \tau_s^{**}}{\partial x_i} - \frac{5}{4}\gamma_5 \tau_s^{**} \frac{\partial \tau_s^{**}}{\partial x_i} + \frac{1}{2}\gamma_3 \frac{\partial^2 u_{iS1}^{**}}{\partial x_j^2}. \tag{9}$$

The modified Knudsen number and normalized parameters are defined as follows:

$$\text{Kn}^{**} = \text{Kn} \frac{\sqrt{\pi}}{2}, \tag{10}$$

$$\tau^{**} = \frac{T}{T_0}, \quad u^{**} = \frac{u}{\sqrt{2RT}}, \quad x = \frac{\bar{x}}{L}. \tag{11}$$

The transport coefficients employed in Eq. (9) depend on gas-molecular models are set to $\gamma_2 = 1.9222, \gamma_3 = 1.9479$, and $\gamma_5 = 0.9611.17$.[36] We compared DSMC and

(a) DSMC heat lines (Kn = 0.1) (b) Heat lines from Eq. (6) (Kn = 0.1)

(c) DSMC heat lines (Kn = 1) (d) Heat lines from Eq. (6) (Kn = 1)
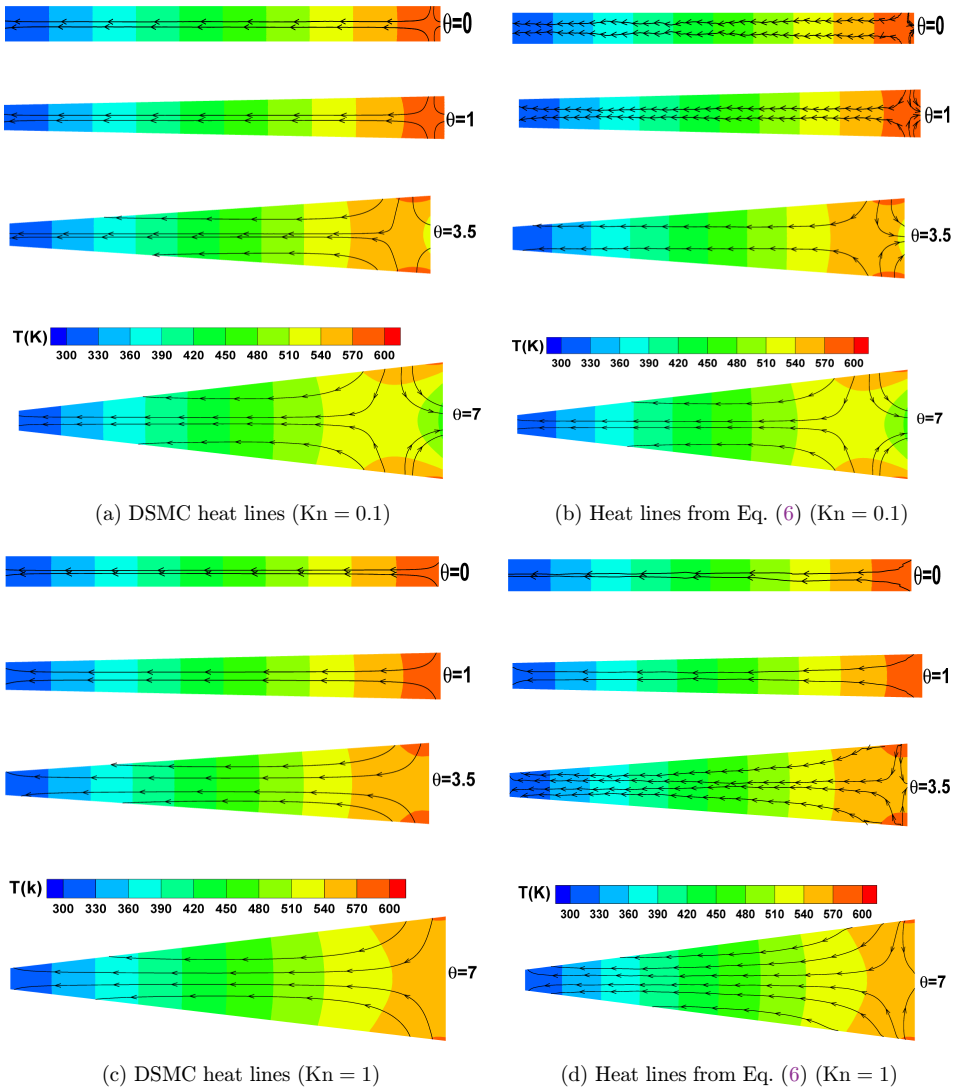
Fig. 12. (Color online) Overall temperature contour with heat lines for (AR = 20, $\Delta T_{\text{wall}}/T_{\text{in}} = 1$).

Sone's predictions at two Knudsen numbers, i.e. Kn = 0.1 and 1, see Fig. 12. The figure indicates that prediction of Sone equations is in good agreement with DSMC solution at Kn = 0.1, however, as Kn approached 1, Sone prediction differed from DSMC's. This is expected because the constitutive relation from the Sone asymptotic theory is for the bulk of the flow and is not expected to predict the gas behavior in the Knudsen layer while at Kn = 1, Knudsen layer occupies almost the entire channel.

5.8. *Effect of divergence angle and AR on normalized thermal mass flow rate*

Thermal creep leads to an induced flow from the cold region to the hot one. Mass flow rate through micro/nanochannels created due to the imposed wall temperature gradient is defined as thermal mass flow rate (M_{th}). Variation of the normalized mass flow rate with the Knudsen number for various wall temperature distributions, aspect ratio, and divergence angle are reported in Figs. 13(a)–13(c). The analytical solution from the asymptotic theory of the Boltzmann equation derived by Ohwada *et al.* and Sone[38,39] and BGK[18] and BKW solution models[40] for straight channel flow are also reported in frames of Fig. 13. The thermal mass flow rate is normalized (M_T) as follows[20]:

$$M_T = \frac{m_{\mathrm{th}}^\cdot}{\rho_{\mathrm{in}}\beta H\sqrt{2RT_{\mathrm{in}}}}. \tag{12}$$

In Eq. (11), β is the normalized temperature gradient multiplied by the channel aspect ratio:

$$\beta = \left(\frac{\Delta T}{T_{\mathrm{in}}}\right)\left(\frac{H}{L}\right), \\ \Delta T_{\mathrm{wall}} = T_{\mathrm{out}} - T_{\mathrm{in}}. \tag{13}$$

The modified inlet Knudsen (K_{in}) is defined as follows:

$$k_{\mathrm{in}} = \frac{\sqrt{\pi}}{2}\mathrm{Kn}_{\mathrm{in}} = \frac{\sqrt{\pi}}{2}\frac{\lambda}{H}. \tag{14}$$

The DSMC results are obtained for channels with AR values of 6 and 20 at different divergence angles. As Fig. 13(a) shows, there is a suitable agreement between the DSMC results and other solutions (asymptotic-BGK-BKW) obtained for small nondimensional temperature gradients ($\Delta T_{\mathrm{wall}}/T_{\mathrm{in}} = 0.02$) while the agreement is not held for higher temperature gradients due to failure of the assumptions behind the derivation of these solutions. On the other hand, our results show that the normalized thermal mass flow rate increases with an increase in the divergence angle and the aspect ratio does not impact mass flow behavior at the bottom border of the
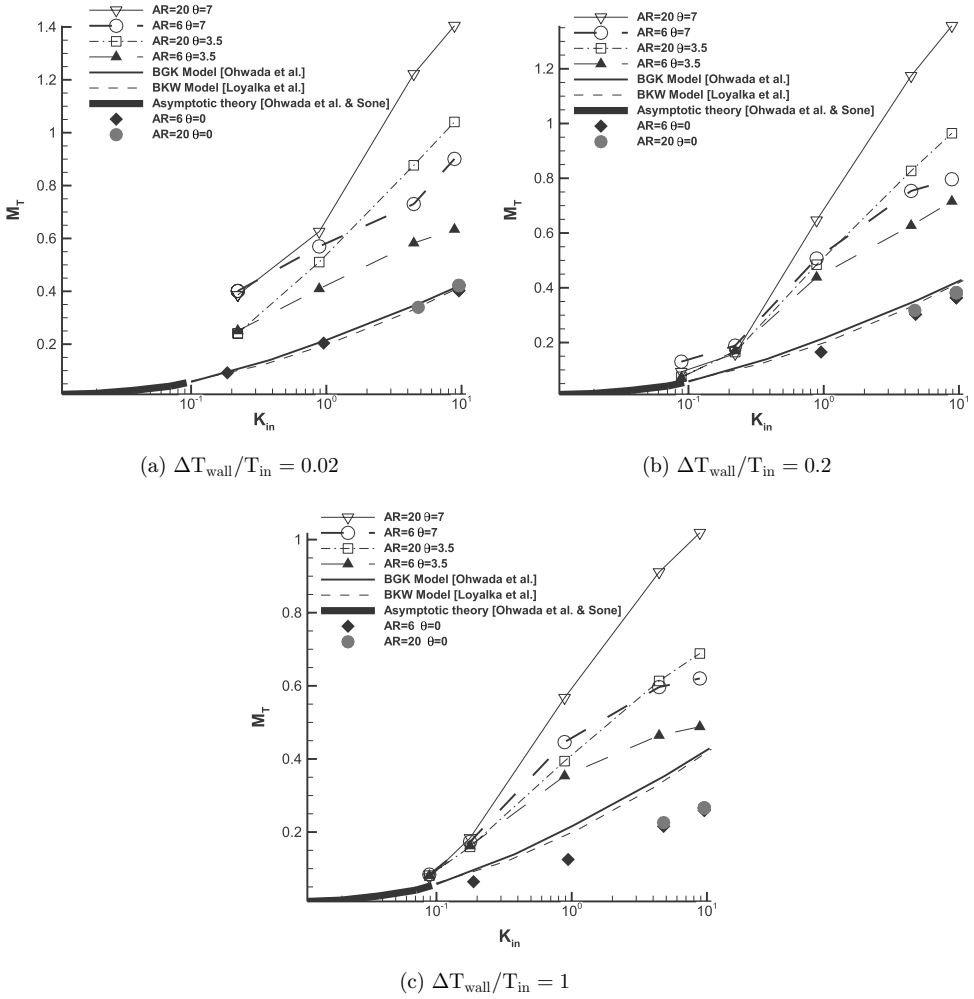
(a) $\Delta T_{\text{wall}}/T_{\text{in}} = 0.02$

(b) $\Delta T_{\text{wall}}/T_{\text{in}} = 0.2$

(c) $\Delta T_{\text{wall}}/T_{\text{in}} = 1$

Fig. 13.   The nondimensional mass flow rate versus k_{in}.

Table 4.   Effect of thermal creep on mass flow rate and nondimensional mass flow rate in divergent micro/nanochannel with $\theta = 3.5$, Kn = 1, AR = 20.

$\Delta T_{\text{wall}}/T_{\text{in}}$	$\dot{m}_{\text{th}} \times 10^{-7}$	$M_T \times 10^{-1}$
0.02	0.129746	5.10556
0.2	1.23072	4.84294
1	5.00715	3.94068

transition regime (Kn = 0.1). However, aspect ratio influences more on the mass flow rate with an increase in the Knudsen number (kn = 1) and for (Kn > 1), its impact is stronger in comparison with the divergence angle on increasing the normalized mass flow rate.

The effect of temperature gradient on the thermal creep mass flow rate (m_{th}) and normalized thermal mass flow rate (M_T) is reported in Table 4. The thermal creep mass flow increases with an increase in the nondimensional temperature due to stronger thermal creep effects while the normalized thermal mass flow rate decreases due to presence of the β term in Eq. (12)

6. Concluding Remarks

In this paper, we investigated thermal creep flow in divergent micro and nano-channels using the particle-based DSMC method. The channel divergence angle changed between 0° and 7° and two aspect ratios (AR = L/H_{in} = 6, 20) were considered. Pressure, Mach number, and magnitude of shear stress distributions were considered at various Knudsen numbers in detail. Our results showed that area expansion effects, specified wall temperature gradient and viscous forces are the parameters influencing the gas fluid behavior in divergent channels. The competition between these parameters could result in a constant Mach number distribution along the channel centerline. Moreover, our results showed the heat flux lines from Sone constitutive equation and the DSMC results are in good agreement at low Knudsen number, i.e. Kn = 0.1. We found that divergence angle could play a significant role in increasing normalized thermal mass flow rate at early transition regime, whereas aspect ratio is more influential on the mass flow rate in comparison with divergence angle at the end of the transition regime.

Acknowledgment

References

1. E. Thielicke and E. Obermeier, *Mechatronics* **10**, 431 (2000).
2. A. S. Holmes, G. Hong, K. R. Pullen and K. R. Buffard, Axial-flow microturbine with electromagnetic generator: Design, CFD simulation, and prototype demonstration. In micro electro mechanical systems, 2004. *17th IEEE International Conference on (MEMS)*, pp. 568–571. IEEE.
3. A. H. Epstein *et al.*, Micro-Heat Engines, Gas Turbines and Rocket Engines-{The MIT} Microengine Project, in *Proc. 28th AIAA Fluid Dynamics Conf.* (1997).
4. A. Agrawal, *Int. J. Micro-Nano Scale Transp.* **2**, 1 (2012).
5. V. S. Duryodhan, S. G. Singh and A. Agrawal, *Microfluid Nanofluid* **38**, 1067 (2013).
6. V. S. Duryodhan, A. Singh, S. G. Singh and A. Agrawal, *Int. J. Heat Mass Transf.* **80**, 424 (2015).

7. V. S. Duryodhan, A. Singh, S. G. Singh and A. Agrawal, A simple and novel way of maintaining constant wall temperature in microdevices. *Scientific Reports* **6**, 18230 (2016).

8. V. S. Duryodhan, S. G. Singh and A. Agrawal, *Int. J. Heat Mass Transf.* **104**, 1022 (2017).

9. V. Varade, V. S. Duryodhan, A. Agrawal, A. M. Pradeep, A. Ebrahimi and E. Roohi, *Comput. Fluids* **111**, 46 (2015).

10. V. Hemadri, V. V. Varade, A. Agrawal and U. V. Bhandarkar, Investigation of rarefied gas flow in microchannels of non-uniform cross section. *Phys. Fluids* **28**(2) (2016) 022007.

11. V. Hemadri, V. V. Varade, A. Agrawal and U. V. Bhandarkar, Rarefied gas flow in converging microchannel in slip and early transition regines. *Phys. Fluids* **29**(3), 32002 (2017).

12. Y. Sone, *Kinetic Theory and Fluid Dynamics*, 1st edn. (Birkhäuser Basel, Birkhäuser Boston, 2002).

13. M. Knudsen, *Kinetic Theory of Gases: Some Modern Aspects* 3rd edn. (Methuen & Co. Ltd., 1950), p. 64.

14. K. Aoki, Y. Sone, Y. Waniguchi and K. Aoki, *Phys. Fluids* **8**(8), 2227 (1996).

15. A. A. Alexeenko, S. F. Gimelshein, E. P. Muntz and A. D. Ketsdever, *Int. J. Therm. Sci.* **45**, 1045 (2006).

16. Y.-L. Han, E. Phillip Muntz, A. Alexeenko and M. Young, *Nanoscale Microscale Thermophys. Eng.* **11**, 151 (2007).

17. S. K. Loyalka, *J. Chem. Phys.* **55**, 4497 (1971).

18. T. Ohwada, Y. Sone and K. Aoki, *Phys. Fluids A* **1**, 2042 (1989).

19. T. Kanki and I. Satoru, *Phys. Fluids* **16**, 938 (1973).

20. H. Akhlaghi and E. Roohi, *Contin. Mech. Thermodyn.* **26**, 67 (2014).

21. G. Tatsios, G. L. Quesada, M. Rojas-Cardenas, L. Baldas, S. Colin and D. Valougeorgis, Computational investigation and parametrization the purping effect in temperature-drive flows through long tapored channels. *Microfluid. Nanofluidics* **21**(5), 99 (2017).

22. G. A. Bird, *Molecular Gas Dynamics and the Direct Simulation of Gas Flows* (Oxford Science, Oxford, 1994).

23. G. A. Bird, *The DSMC Method* (CreateSpace Publisher, USA, 2013).

24. C. Shen, *Rarefied Gas Dynamics: Fundamentals, Simulations and Micro Flows* (Springer Science & Business Media, Berlin, 2006).

25. E. Roohi and S. Stefanov, *Phys. Rep.* **656**, 1 (2016).

26. H. Akhlaghi, E. Roohi and S. Stefanov, *Comput. Fluids* **161**, 23 (2018).

27. E. Roohi, S. Stefanov, A. Shoja-Sani and H. Ejraei, *J. Comput. Phys.* **354C**, 476 (2018).

28. A. Shoja-Sani, E. Roohi, M. Kahron and S. Stefanov, *European Journal of Mechanic Part B: Fluids*, **48**, 59 (2014).

29. T. J. Scanlon, E. Roohi, C. White, M. Darbandi and J. M. Reese, *Comput. Fluids* **39**, 2078 (2010).

30. C. White, M. K. Borg, T. J. Scanlon and J. M. Reese, *Comput. Fluids* **71**, 261 (2013).

31. C. White, M. K. Borg, T. J. Scanlon, S. M. Longshaw, B. John, D. R. Emerson and J. M. Reese, *Comput. Phys. Commun.* Published online (2017). Yet in press: http://www.sciencedirect.com/science/article/pii/S0010465517303375.

32. C. Shu, X. H. Mao and Y. T. Chew, *Int. J. Numer. Methods Heat Fluid Flow* **15**, 827 (2005).

33. G. A. Bird, *Sophisticated DSMC, Notes Prepared for a Short Course at the DSMC07meeting* (Santa Fe, USA; 2007).

34. Z. X. Sun, Z. Tang, Y. L. He and W. Q. Tao, *Comput. Fluids* **50**, 1 (2011).

35. W. Liou and Y. Fang, *Microfluid Mechanics: Principles and Modeling* (Mcgraw-hill, 2005), p. 350.

36. Y. Sone, *Molecular Gas Dynamics: Theory, Techniques, and Applications*, 1st edn. (Birkhäuser Basel, Birkhäuser Boston, 2007).

37. H. R. Van Den Berg, C. A. Seldam and P. S. Van Der Gulik, **14**, 4 (1993).

38. Y. Sone and K. Aoki, *Mem. Fac. Eng., Kyoto Univ.* **49**, 237 (1987).

39. T. Ohwada, Y. Sone and K. Aoki, *Phys. Fluids A Fluid Dyn.* **1**, 363 (1989).

40. S. K. Loyalka, *Phys. Fluids* **17**, 1053 (1974).